JCI The Journal of Clinical Investigation

Stromal epigenetic alterations drive metabolic and neuroendocrine prostate cancer reprogramming

Rajeev Mishra, … , Edwin M. Posadas, Neil A. Bhowmick

J Clin Invest. 2018. https://doi.org/10.1172/JCI99397.

Research In-Press Preview **Cell biology** **Metabolism**

Prostate cancer is an androgen-dependent disease subject to interactions between the tumor epithelia and its microenvironment. Here, we found epigenetic changes in cancer-associated prostatic fibroblasts (CAF) initiated a cascade of stromal-epithelial interactions. This facilitated lethal prostate cancer growth and development of resistance to androgen signaling deprivation therapy (ADT). We identified that a Ras inhibitor, *RASAL3*, is epigenetically silenced in human prostatic CAF, leading to oncogenic Ras activity driving macropinocytosis-mediated glutamine synthesis. Interestingly, ADT further promoted *RASAL3* epigenetic silencing and glutamine secretion by prostatic fibroblasts. In a orthotopic xenograft model, subsequent inhibition of macropinocytosis and glutamine transport resulted in antitumor effects. Stromal glutamine served as a source of energy through anaplerosis and as a mediator of neuroendocrine differentiation for prostate adenocarcinoma. Antagonizing the uptake of glutamine restored sensitivity to ADT in a castrate resistant xenograft model. In validating these findings, we found that prostate cancer patients on ADT with therapeutic resistance had elevated blood glutamine levels compared to those with therapeutically responsive disease (odds ratio = 7.451, $P = 0.02$). Identification of epigenetic regulation of RAS activity in prostatic CAF revealed RASAL3 as a sensor for metabolic and neuroendocrine reprogramming in prostate cancer patients failing ADT.

Stromal epigenetic alterations drive metabolic and neuroendocrine prostate cancer reprogramming

Rajeev Mishra[1], Subhash Haldar[1], Veronica Placencio[1], Anisha Madhav[2], Krizia Rohena-Rivera[1], Priyanka Agarwal[1], Frank Duong[1], Bryan Angara[1], Manisha Tripathi[1], Zhenqiu Liu[1], Roberta A. Gottlieb[2], Shawn Wagner[2], Edwin M. Posadas[1], Neil A. Bhowmick[1,2,3]

[1] Department of Medicine, Cedars-Sinai Medical Center, Los Angeles, CA, USA

[2] Department of Biomedical Sciences, Cedars-Sinai Medical Center, Los Angeles, CA, USA

[3]Department of Research, Greater Los Angeles Veterans Administration, Los Angeles, CA, USA

*Correspondence to:

Neil A. Bhowmick, Ph.D.

Cedars-Sinai Medical Center,

8750 Beverly Blvd. Atrium 103, Los Angeles, CA 90048, USA.

Tel: 1-310-423-5589, Fax: 1-310-423-8543, E-mail: bhowmickn@cshs.org

Conflict of interest: The authors have declared that no conflict of interest exists.

Abstract

Prostate cancer is an androgen-dependent disease subject to interactions between the tumor epithelia and its microenvironment. Here, we found epigenetic changes in cancer-associated prostatic fibroblasts (CAF) initiated a cascade of stromal-epithelial interactions. This facilitated lethal prostate cancer growth and development of resistance to androgen signaling deprivation therapy (ADT). We identified that a Ras inhibitor, *RASAL3*, is epigenetically silenced in human prostatic CAF, leading to oncogenic Ras activity driving macropinocytosis-mediated glutamine synthesis. Interestingly, ADT further promoted *RASAL3* epigenetic silencing and glutamine secretion by prostatic fibroblasts. In an orthotopic xenograft model, subsequent inhibition of macropinocytosis and glutamine transport resulted in antitumor effects. Stromal glutamine served as a source of energy through anaplerosis and as a mediator of neuroendocrine differentiation for prostate adenocarcinoma. Antagonizing the uptake of glutamine restored sensitivity to ADT in a castrate resistant xenograft model. In validating these findings, we found that prostate cancer patients on ADT with therapeutic resistance had elevated blood glutamine levels compared to those with therapeutically responsive disease (odds ratio = 7.451, $P = 0.02$). Identification of epigenetic regulation of Ras activity in prostatic CAF revealed *RASAL3* as a sensor for metabolic and neuroendocrine reprogramming in prostate cancer patients failing ADT.

Introduction

Despite improved detection and therapies nearly 30,000 men continue to die of prostate cancer (PCa) in the United States and over 300,000 globally (1, 2). Currently, all therapeutic approaches for metastatic PCa involve interference of androgen signaling, however none are curative. Examination of mechanisms of androgen signaling deprivation therapy (ADT) resistance point to a cell autonomous process associated with expansion of a resistant clonal population as other sensitive cells die off and an adaptation process, where stromal and epithelial cells co-evolve to support tumor survival. The cell autonomous processes can be a direct result of spontaneous somatic mutations favorable for an androgen deprived environment. Evidence for stromal changes induced by ADT is associated with expression of paracrine growth factors in support of stromal-epithelial adaptation to therapeutic pressures (3, 4). The autocrine and paracrine processes are not mutually exclusive. Although prostate cancer associated fibroblasts (CAF) are not subject to somatic mutations, epigenetic changes are documented and attributed to the prediction of disease progression (5-7). We functionally differentiate CAF from their counterpart, normal associated fibroblasts (NAF), as cells that can induce tumorigenesis in non-tumorigenic prostatic epithelia. NAF, also derived from prostatectomy tissues, are unable to induce tumorigenesis, as Cunha and colleagues have previously described (8, 9). Interestingly, the expression patterns of oncogenes and tumor suppressors in CAF have emerged as tumor promoting and tumor inhibitory, respectively. As an example, loss of the tumor suppressors phosphatase and tensin homolog (*PTEN*) and the transforming growth factor-ß receptor type II (*TGFBR2*), in fibroblastic cells are tumorigenic in breast and prostate cancer (10-12). Similarly, the expression of oncogenes, cyclin D1 (*CCND1*) and *CMYC*, in the CAF has been associated with its tumorigenicity in prostate cancer (13-15). Here, we explored how epigenetic changes can mediate oncogenic signaling in CAF and epithelial metabolic reprogramming.

Stromal-epithelial interactions can dictate cancer progression, differentiation, and even therapeutic responsiveness. The high glucose consumption of cancer cells described for many cancers is not commonly

observed in PCa, as lactate generated by CAF is an important source of energy in disease progression through a familiar reverse Warburg process (16, 17). Interestingly, pancreatic cancer epithelia are prominently found to engulf extracellular material through a process of macropinocytosis to generate glutamine through lysosomal breakdown of serum components. Macropinocytosis is the result of activated Ras signaling endemic to pancreatic cancer, where the glutamine generated is taken up by neighboring cells, serving to support active TCA cycle activity (18, 19). Ras family proteins are small GTPases that cycle between the inactive GDP-bound and activated GTP-bound states. This cycling occurs with the help of guanine nucleotide exchange factors (RasGEFs) that promote activation, and GTPase-activating proteins (RasGAPs) that inactivate Ras by catalyzing GTP hydrolysis. Although Ras mutations are common oncogenic drivers in many cancer types, these are infrequent in prostate tumor cells. We identified role of Ras signaling-mediated macropinocytosis in PCa.

Oncogenic Ras promotes metabolic reprogramming of cancer epithelia by enhancing glucose uptake, glycolytic activity, and a shift to glutamine metabolism in a cell autonomous manner. Glutamine is considered a conditionally essential amino acid, particularly for cells under stressed conditions, like cancer. To maintain tumor growth, the carbon and nitrogen from glutamine become essential for active biosynthesis. The additional conversion of glutamine to glutamate, available through glutaminase activity (GLS and GLS2), can support the high energy needs of cancer cells, as its subsequent metabolism to α-ketoglutarate is an entry point for the TCA cycle and oxidative phosphorylation. Elevated blood glutamate is reported to be associated with higher grade PCa (20). Nevertheless, the role of glutamine/glutamate in energetics and cellular biomass does not seem to address its association with tumor aggressiveness. It is not clear if ADT is selective or causative of aggressive recurrent PCa. Our study explores the expanding role of ADT on stromal epigenetic changes and paracrine glutamine signaling contributing to epithelial therapeutic resistance.

Results

DNA methylome analysis revealed epigenetic silencing of RASAL3 in prostatic CAF. To identify differences in the methylation status of prostate fibroblasts from human benign and PCa tissues, we performed whole-genome methylation analysis by Reduced Representation Bisulfite Sequencing (RRBS). To determine differentially methylated CpG sites, we analyzed, in a pairwise fashion, sequencing data from 10 primary prostatic NAF and CAF samples. The RRBS analysis led to a list of more than 2000 genes that displayed differential promoter methylation in the NAF and CAF populations (Supplemental Table 1). Among the top 20 hypermethylated promoters in CAF, four genes appeared to top the list and were tested: *CD74*, *RASAL3*, *B3GNT1*, and *NTRK1* (Figure 1A and Supplemental Figure 1A). Out of the four genes, *CD74*, *NTRK1* (Neurotrophic Receptor Tyrosine Kinase 1), and *B3GNT1* (Beta-1,4-Glucuronyltransferase 1), part of glycosaminoglycan metabolism pathway, have established roles in promoting tumor progression (21-23). However, the RasGAP, RASAL3 (RAS protein activator like 3), a Ras signaling antagonist, located at the 19p13.12 locus demonstrated exon 2 hypermethylation in CAF ($P < 0.002$; Figure 1, B and C) has not been studied with respect to its role in tumor progression. We selected *RASAL3* as a candidate gene for further study, as promoter hypermethylation and silencing of a tumor suppressor in CAF may have a tumorigenic effect.

To confirm the methylation status of the *RASAL3* promoter, methylation-specific PCR and bisulfite genomic sequencing were performed in NAF and CAF primary lines. Greater exon 2 methylation was found in the CAF compared to the NAF, as determined by methylation-specific PCR (Supplemental Figure 1B). Bisulfite sequencing of exon 2 demonstrated 73.3% CpG dinucleotide methylation of *RASAL3* in CAF, compared to 37.1% CpG methylation in NAF, confirming the methylome analysis (Figure 1B). Accordingly, *RASAL3* mRNA expression was found to be significantly downregulated in CAF from five patients compared to NAF from three patients, as determined by quantitative-rtPCR (Figure 1D). However, Oncomine analysis demonstrated no significant difference in *RASAL3* expression in normal and PCa tumor tissues from either PRAD/Broad and

Taylor data sets (Figures 1, E and F). *RASAL3* was prominently epigenetically silenced in human CAF compared to NAF, but is not differentially expressed in the epithelial compartment, enriched in the two data sets.

Ras signaling activation in prostatic fibroblast leads to macropinocytosis. Since the RasGAPs are negative regulators of Ras and their loss contributes to Ras pathway activation, we tested Ras activity in CAF and NAF. We found that RASAL3 protein expression was reduced in a primary CAF population, accompanied by a substantial increase in Ras-GTP (active Ras), phosphorylated-c-Raf, phosphorylated-ERK, compared to that in NAF (Figure 2A). Total Ras and cRaf protein expression remained unchanged in NAF and CAF. We reasoned that the role of epigenetically-induced Ras activation in CAF could trigger an endocytic process of macropinocytosis similar to that reported in pancreatic cancer epithelia (18). The uptake of fluorescent dextran beads (TMR-70kDa dextran) in NAF and CAF populations were visualized. Interestingly, dextran labeling experiments illustrated a large number of macropinosomes in CAF, with no detectible uptake of fluorescence in the NAF (Figure 2B). TMR-dextran uptake by CAF was inhibited by the macropinocytosis inhibitor, 5-(N-Ethyl-N-isopropyl) amiloride (EIPA), as well as the DNA demethylase, 5-aza-2'-deoxycytidine, in support of epigenetic regulation of macropinocytosis in these fibroblasts (Supplemental Figure 2A). We further found that macropinosomes in CAF trafficked to lysosomes while undergoing a process of maturation characterized by vesicular size reduction concomitant with membrane fusion visualized by co-localization of TMR-dextran and lysotracker (Supplemental Figure 2B). To identify albumin proteolysis in CAF, we used self-quenching BODIPY dye conjugated to BSA (DQ-BSA) that emits green fluorescence following proteolytic digestion. The co-localization of TMR-dextran and DQ-BSA indicated degraded BSA was compartmentalized in macropinocytic vesicles within CAF (Figure 2C). The epigenetic silencing of *RASAL3* in CAF correlated with Ras-mediated macropinocytosis and subsequent degradation of BSA.

To directly determine if Ras signaling confers a tumor supportive role associated with CAF, we used CRISPR/Cas9 to knock out *Rasal3* in mouse prostatic fibroblasts. Compared to the expression of Cas9 fibroblasts (control), Ras activity and ERK phosphorylation was elevated in Rasal3-knockout (Rasal3-KO) fibroblasts (Figure 2D). Rasal3-KO fibroblasts took up TMR dextran, whereas it was undetectable in the control fibroblasts (Figure 2E). The exogenous expression of active Ras^{V12} (Gly^{12}→Val^{12}) in wild-type mouse prostatic fibroblasts replicated the downstream ERK activation and macropinocytosis observed in CAF and Rasal3-KO cells (Figure 2 F,G). Thus, epigenetic *RASAL3* silencing of prostatic fibroblasts promoted familiar signaling and macropinocytosis associated with Ras transformation (18). Conversely, PCa epithelial cell lines, CWR22Rv1 and C4-2B, were not found to exhibit macropinocytosis, based on TMR-dextran uptake (Supplemental Figure 2C). To test the role of stromal Ras-mediated macropinocytosis on tumor development, orthotopic PCa xenograft models were used. Tissue recombinants of Ras^{V12}-expressing fibroblasts and CWR22Rv1 epithelia were grafted into the anterior prostates of SCID mice. Two weeks later, mice were treated with vehicle control or EIPA for 1 week to suppress macropinocytosis (Figure 2H). We found that the mice treated with EIPA had dramatically reduced tumor size with respect to the control group. Treatment with EIPA had no significant effect on the viability of the CWR22Rv1 or wild type fibroblasts, but EIPA reduced the viability of the Rasal3-KO fibroblasts ($P < 0.001$, Supplemental Figure 3A). Thus, glutamine uptake by the tumor was necessary for its expansion.

Uptake of fibroblast-derived glutamine by prostate cancer epithelia impacts its metabolism.

To establish the role of Ras on the reactive properties of fibroblasts, we tested its role on the expression of a panel of CAF-defining genes. Ras^{V12}-fibroblasts had 2.5- to 140-fold elevated expression of a panel of CAF marker-genes, compared to wild type fibroblasts, inclusive of tenascin C, FAP, MMP1a, and MMP3 (two-way ANOVA $P < 0.0001$, Figure 3A). Because reactive fibroblasts are recognized to potentiate adjacent epithelial expansion, epithelial proliferation was tested in three-dimensional (3D) co-cultures with fibroblasts. PCa epithelia, CWR22Rv1 and C4-2B, were found to be significantly more proliferative when cultured with Ras^{V12}-

fibroblasts, compared to wild type fibroblasts (Figure 2B, Supplemental Figure 3B). To determine if a soluble factor was involved in the paracrine process, a transwell assay was performed with Cas9 or Rasal3-KO fibroblasts in the upper chamber and CWR22Rv1 in the lower well (Supplemental Figure 3C). We found a significant proliferative induction of the epithelia when associated with Rasal3-KO fibroblasts, compared to Cas9 control fibroblasts. To correlate the uptake of albumin in fibroblasts and elevated Ras activity with epithelial proliferation we tested whether the stromal media affected epithelial ATP generation. Conditioned media (CM) from both Ras^{V12}-fibroblast induced ATP production in CWR22Rv1 and C4-2B, over CM from the wild type counterpart (Figure 3C, Supplemental Figure 4A). Similar ATP generation was observed in CWR22Rv1 in the context of CAF-CM, compared to NAF-CM. The ATP synthase inhibitor, oligomycin, served as the negative control for ATP detection. These results suggested that Ras-induced macropinocytosis in stromal fibroblasts confer a change in tumor-energy metabolism via a paracrine soluble factor.

As it was clear that epigenetically transformed stromal fibroblasts provided the energy needs of the epithelia, the nature of these metabolic changes was explored. Metabolome analysis of CWR22Rv1 demonstrated glutamine and glutamate to be significantly elevated when exposed to CAF-CM, compared to NAF-CM, ($P < 0.01$, Figure 3D). This was consistent with macropinocytosis of albumin, as previously reported in pancreatic cancer (24). Consequently, succinate, fumarate and malate levels were significantly elevated in the CAF-CM treated group, compared to that induced by NAF-CM, consistent with glutamine metabolism. However, there was no significant difference in the levels of acetyl-CoA, α-ketoglutarate, and 2-hydroxyglutarate, but decreased levels of citrate in the epithelia treated with CM from CAF compared to NAF. The lack of a difference in α-ketoglutarate levels could be a result of increased flux to its metabolites (i.e. succinate, fumarate, malate). Further, there was an observed increase in levels of the nucleotide precursor aspartate ($P < 0.05$) and oxidized-GSH ($P < 0.01$), metabolites which are downstream of glutamate metabolism (Figure 3E). CAF-CM, compared to NAF-CM did not significantly

change reduced-GSH levels, associated with increased mitochondrial activity and reactive oxygen in cancer cells.

In agreement with past reports of macropinocytosis-induced glutamine generation (18, 25), we found that like the CAF, Rasal3-KO and Ras^{V12}-mouse fibroblasts secreted significantly more glutamine into the media than their NAF or wild type counterparts (Figure 3F, Supplemental Figure 4B). To support the role of stromal-derived glutamine on epithelial proliferation, we supplemented 0.4 mM glutamine to NAF-CM, to find it restored CWR22Rv1 proliferation to that similar to CAF-CM, based on direct measurement of glutamine generated by CAF (Figure 3G). Developments in magnetic resonance imaging technology have enabled glutamine/glutamate imaging with improved spatial and temporal resolution. However, its application has been relegated to glioblastoma/medulloblastoma imaging, as they are commonly Ras-driven cancers with abundance of glutamine and glutamate in the tissue (25-27). We were able to identify the presence of glutamine/glutamate in a tissue recombination xenograft model of CWR22Rv1 and Ras^{V12}-mouse fibroblasts. To validate the specificity of the glutamine/glutamate signal, macropinocytosis was inhibited by administering EIPA to the mice and re-imaged (using simulated echo acquisition, Figure 3H). Stromal fibroblastic Ras driven-macropinocytosis results in glutamine production and utilized by cancer epithelia to promote its expansion.

To corroborate the observed epithelial accumulation of glutamine and its downstream metabolites, we tested if CAF-CM regulated the expression of amino acid transporters and glutaminase expression in CWR22Rv1 and C4-2B cells. Specifically, the glutamine importer *SLC1A5* mRNA expression was upregulated in CWR22Rv1 ($P < 0.0001$) and C4-2B ($P < 0.001$) by CAF-CM, compared to NAF-CM (Supplementary Figure 4C). Supplementing basal media with L-glutamine consistently increased the expression of glutamine importers *SLC1A5* and *SCL38A2*, in both CWR22Rv1 and C4-2B cells in a time dependent manner (Supplemental Figure 4D-G). While, the *SLC38A1* transporter did not seem to be regulated by exogenous glutamine in either epithelial line,

CWR22Rv1 cells expressed *SLC38A4* in a glutamine dependent manner. Once the glutamine enters the epithelia, it can undergo anaplerosis by which glutamine is converted to glutamate by glutaminase (i.e. *GLS* or *GLS2*) to replenish the TCA cycle. Glutamine uptake was able to promote both *GLS* and *GLS2* mRNA expression within 6 hours of treatment in C4-2B cells (Supplemental Figure 4H). We found *GLS* mRNA expression level was also elevated in the CAF-CM treated group compared with NAF-CM treated group in both CWR22Rv1 ($P < 0.0001$) and C4-2B ($P < 0.01$) cells (Supplemental Figure 4I). *GLS2* mRNA expression was however downregulated in CWR22Rv1 cell ($P < 0.001$) and upregulated in C4-2B cells ($P < 0.0001$) by CAF-CM treatment when compared to NAF-CM treatment (Supplemental Figure 4J). These data demonstrated that glutamine taken up by the epithelia are metabolized through a seemingly positive feedback mechanism to support the elevated energy needs of cancer epithelia (Supplemental Figure 4J).

We found that glutamine uptake provided energy and mediated differentiation signaling for the prostatic epithelia. The prostatic CAF potentiated epithelial TCA flux resulting in a mitochondrial response in CWR22Rv1 cells, by the administration of exogenous glutamine (Figure 4A). Similarly, Ras^{V12}-fibroblast-CM upregulated basal oxygen consumption, ATP generation, and maximal mitochondrial respiration in CWR22Rv1 and C4-2B, compared to that with wild type fibroblast-CM (Figure 4B, Supplemental Figure 5A). Glutamine deprivation by treatment with an SLC1A5 inhibitor, L-γ-glutamyl-p-nitroanilide (GPNA) on CWR22Rv1 and C4-2B in the context of Ras^{V12} fibroblast-CM, restored basal respiration, ATP, and maximal respiration to that observed with wild type fibroblast-CM. To determine the impact of stromal-derived glutamine on epithelial proliferation, we blocked glutamine uptake and utilization with selective inhibitors in 3D co-cultures of primary human CAF and CWR22Rv1 cells. We found that blocking SLC1A5 (i.e., GPNA) and GLS (i.e., bis-2-[5–phenylacetamido-1, 2, 4-thiadiazol-2-yl] ethyl sulfide: BPTES) function significantly decreased epithelial proliferation, as determined by quantitating Ki-67 staining of $EpCAM^+$ cells through FACS analysis ($P < 0.05$ and $P < 0.001$, respectively, Figure 4C). Thus, the stromal epigenetic modification resulted in glutamine production for the maintenance of ATP

levels and proliferation in cancer cells. Given that mTOR is a nutrient sensor for glutamine, we reasoned that the same pathway may affect mechanisms of prostate cancer differentiation (28, 29). We found mTOR to be activated in CWR22Rv1 cells incubated with Ras^{V12}-fibroblast-CM (Figure 4D; Statistical analysis shown in Supplementary Table 2). Moreover, expression of Forkhead box M1 (FOXM1), a key signal downstream of mTOR and a critical transcription factor in multiple poorly differentiated cancer types (30-32) was upregulated in CWR22Rv1 cells incubated with Ras^{V12}-fibroblast-CM. FOXM1 was also found to interact with multiple neuroendocrine differentiation factors as shown by STRING analysis (Figure 4E) (33). Remarkably, the incubation of CWR22Rv1 cells with Ras^{V12}-fibroblast-CM resulted in significant increase in neuroendocrine differentiation genes shown in a heatmap (F-test $P < 0.0001$, Figure 4F). Similarly, the addition of L-glutamine alone upregulated a panel of neuroendocrine gene panel in CWR22Rv1 epithelia (F-test $P < 0.0001$), with the inhibition of mTOR by rapamycin restoring its expression to control levels (Figures 4G). The sufficiency for glutamine alone to induce neuroendocrine differentiation was further confirmed in C4-2B cells ($P < 0.0001$, Supplemental Figure 5B). Finally, we found that the knockdown of either SLC1A5 or GLS by siRNA was able to reverse the effect of glutamine-induced neuroendocrine differentiation of CWR22Rv1 (Supplemental Figure 5C). Taken together, these results demonstrated that stromal glutamine was sufficient and necessary for epithelial proliferation and differentiation to a more aggressive PCa phenotype mediated by stromal Ras activity.

Epigenetic alteration of RASAL3 mRNA expression by androgen signaling affects glutamine driven tumor progression. Neuroendocrine PCa is rare, however neuroendocrine differentiation is more commonly observed as a potential adaptive response to newer, more potent ADT (34). To explore the possible involvement of androgen signaling on prostatic stromal epigenetic alteration, we initially measured *RASAL3* mRNA expression in the context of androgen and androgen receptor antagonists. As before, we found that NAF populations had greater *RASAL3* mRNA expression compared to CAF (Figure 5A, Supplemental Figure 6A). The treatment with the stable androgen analog, R1881, had no effect on *RASAL3* mRNA expression level in

NAF; however, it significantly elevated *RASAL3* mRNA expression in CAF. Conversely, androgen receptor antagonists, bicalutamide and enzalutamide, downregulated *RASAL3* mRNA expression in NAF, yet had little effect on the already low basal mRNA expression of *RASAL3* in the CAF. As evidence of epigenetic alteration of CAF by androgen signaling, we found that the demethylating agent, 5-aza-2'-deoxycytidine, restored *RASAL3* mRNA expression in CAF, similar to that found by R1881. The expression data was supported by methylation specific PCR demonstrating the hypermethylation of the *RASAL3* promoter by bicalutamide and enzalutamide and hypomethylation by R1881, similar to 5-aza-2'-deoxycytidine treatment (Supplemental Figure 6B). To quantitate methylation status of the *RASAL3* exon 2 region we performed bisulfite sequencing of CAF treated with R1881. Androgen signaling was found to prevent CpG methylation of *RASAL3*, by 2.6-fold over the vehicle treated CAF (Figure 5B).

To determine the role of resulting glutamine on neuroendocrine differentiation, 3D co-cultures of CAF-CWR22Rv1 were treated with glutamine uptake or conversion blockers, GPNA or BPTES, in the context of enzalutamide. The administration of either BPTES or GPNA significantly reduced the mRNA expression of the panel of neuroendocrine biomarker genes, well below control levels (F test $P < 0.0001$, Figure 5C). As neuroendocrine differentiation can potentiate PCa castrate resistance, in the next set of mouse studies, we tested the role of glutamine uptake on tumor expansion. In tissue recombinant xenograft models, mice were either left intact or castrated, then treated with enzalutamide, followed by administration of vehicle or GPNA, as outlined in Figure 5D and Supplemental Figure 7A. In intact mice, the administration of GPNA resulted in reduced tumor volume ($P < 0.001$) and mitotic index, as determined by phosphorylated-histone H3 immunolocalization ($P < 0.0001$, Supplemental Figure 7B-D). In the castrated, enzalutamide treated mice, we found that these tissue recombinant tumors expanded despite ADT, but the added treatment with GPNA significantly reduced tumor size (Figure 5E, F; $P < 0.0001$). Histological analysis revealed ADT resulted in solid sheets of cells, whereas addition of GPNA treatment was associated with karyolytic cells (Figure 6A). In agreement with the results of the

neuroendocrine gene panel, GPNA treatment reduced chromogranin A expression induced by castration and enzalutamide treatment. Accordingly, the localization of phosphorylated-mTOR (Ser-2481) was reduced ($P < 0.05$) and cell death (TUNEL, $P < 0.001$) was elevated by the combination treatment, compared to ADT alone (Figure 6B). However, blocking both androgen signaling and glutamine uptake did not significantly change the mitotic index of the tumors, compared to androgen signaling blockage alone, as localized by phosphorylated histone H3 staining. These data argue that using ADT potentiates glutamine expression by prostatic fibroblasts via *RASAL3* epigenetic silencing and limiting the uptake of glutamine by the epithelia can curb the ramifications of stromal Ras activity, including the support of the epithelial energy needs and neuroendocrine differentiation.

Plasma glutamine level may be prognostic for ADT sensitivity. Considering the striking finding that glutamine can induce ADT resistance, we tested if glutamine concentrations can be associated with ADT sensitivity in prostate cancer patients. We measured blood plasma glutamine concentrations in 28 PCa patients that received ADT (Table 1). Of note, the specific androgen signaling-axis interventions in the patient pool included, androgen receptor antagonists: bicalutamide, enzalutamide, and apalutamide, as well as androgen synthesis inhibitors: leuprolide, goserelin, triptorelin, and abiraterone. Of the samples analyzed, 18 patients were responsive and 10 were not responsive to ADT, based on serum prostate specific antigen (PSA) regulation (Figure 7A). The waterfall plot illustrates patients with glutamine concentrations above 2 mM corresponded to disease progression on ADT and those with glutamine values at or below the threshold to be treatment-responsive (Fisher exact test odds ratio of 7.451, $P = 0.02$). Compared to baseline glutamine concentrations of 0.4-0.7 mM in normal subjects, the PCa patients in this small cohort overall had markedly elevated glutamine concentrations (average = 1.8 mM), in agreement with previously reported elevations in glutamate levels in high grade PCa subjects (20). These results support the concept that reduced ADT-sensitivity is associated with elevated circulating glutamine concentrations.

Discussion

This study reports that ADT can induce epigenetic alteration of the stromal fibroblasts to promote PCa progression to a more aggressive differentiation state. Based on our earlier report that prostatic CAF have elevated DNA hypermethylation due to epithelia-derived paracrine signals (6), we performed a whole genome methylome analysis to reveal the silencing of a tumor suppressor, RASAL3. The outcomes of our interrogation of stromal-epithelial interactions are summarized in Figure 7B, where the hypermethylation of the *RASAL3* promoter in CAF induced RAS-dependent macropinocytosis for the lysosomal catabolism of albumin and generation of glutamine. Metabolomic profiling uncovered the role of stromal glutamine as an underlying metabolic controller facilitating cell survival and proliferation. Glutamine transporter-facilitated uptake and subsequent metabolism of stromal glutamine into epithelia for utilization by the TCA cycle and mTOR activation contribute to the energy needs of the cancer and its differentiation, respectively. This is the first demonstration of epigenetic Ras regulation in CAF consequently contributing to cancer progression. Targeting Ras signaling via RasGAPs, has been a focus of many laboratories. We demonstrated that human CAFs have low expression of *RASAL3*, due to exon 2 hypermethylation, resulting in Ras signaling activation. We further found that elevated Ras activity in prostatic mouse wild type fibroblasts was sufficient to promote differentiation state analogous to the tumor promoting CAF (8, 9). Others have identified epigenetic silencing of RASAL isoforms associated with aberrant Ras activation in cancer epithelial subtypes (35, 36). *RASAL1* hypermethylation, mediated by DNMT1, is also reported to promote renal fibrosis (37). Our findings provide evidence for RasGAP gene methylation and Ras signaling in CAF. Silencing of *RASAL3* contributed to downstream cRaf and ERK activation in the absence of a change in Ras expression. So, the common loss of PTEN expression in PCa epithelia, is not necessarily the only determinant for elevated PI3 kinase activity in tumor tissues (38).

A key finding of the present work adds a dimension to the previously recognized epigenetic regulation by androgen signaling. Gravina et al., showed that androgen receptor is a key regulator of DNMT expression in

some PCa cell models (39). They demonstrated that PCa epithelia treated with bicalutamide or cultured in androgen-depleted medium progressively acquire greater DNA methyltransferase (DNMT) activity compared to cells cultured under standard conditions. Conversely, 10^{-12} M dihydrotestosterone was able to reduce DNMT activity. As prostatic fibroblasts also express androgen receptor (40, 41), it was consistent with the observed RASAL3 promoter hypermethylation (Fig. 5). The subsequent activation of Ras signaling suggested the testing of macropinocytosis, based on the seminal identification of this process in pancreatic cancer with high Ras mutation frequency (18). The knockout of Rasal3 and overexpression of Ras^{V12} in wild type mouse prostatic fibroblasts recapitulated the observation of macropinocytosis strikingly prevalent in primary human prostatic CAF derived from multiple patient tissues (Figures 1, 2). Uniquely, the activation of Ras signaling in prostatic fibroblasts demonstrated elevated expression of a gene panel associated with a reactive fibroblastic state. This was not entirely surprising since we and others have previously demonstrated the downregulation of tumor suppressors (*e.g. TGFBR2, PTEN*) and upregulation of oncogenes (*e.g. MYC, CCND1*) in the CAF to have pro-tumorigenic capacity (10, 11, 13-15). What was not predicted, however, was that androgen deprivation further silenced *RASAL3* in NAF and was coincident with acquisition of the CAF features (Figures 3, 5). Thus, epigenetic modification of tumor associate fibroblasts can be initiated by ADT, and extraordinarily be a mechanism of resistance to ADT in a paracrine manner.

Cancer cells survive and even thrive under hypoxic and in what is thought to be nutrient deprived conditions. However, glutamine, a conditionally essential amino acid most commonly depleted amino acid in solid tumors, can serve as a carbon source for TCA cycle and as a nitrogen source for nucleotide biosynthesis (42). Like glucose, amino acids cannot cross the lipid bilayer without transporter proteins, and amino acid transporter expression is positively correlated with growth and cancer (43). We found the expression level of glutamine transporters and glutaminase in CWR22RV1 and C4-2B cells are potentiated by glutamine secreted from CAF, allowing its own uptake (Supplemental Figure 4). Within the epithelia, glutamine conversion to glutamate could

be metabolized into α-ketoglutarate, aspartate, and glutathione (Figure 3). The lack of observed α-ketoglutarate accumulation was likely due to its oxidation to succinate, fumarate, and malate to address the energy needs by oxidative phosphorylation. However, glutamate conversion to significantly elevated oxidized glutathione was further indication of accumulated oxidative stress mediated by active mitochondrial electron transport (44). The prominent levels of the glutamine-derivative, aspartate, found in the epithelia when exposed to CAF is a key oxidized precursor for both purines and pyrimidines further support cell proliferation (45). Thus, the androgen-dependent switch of the tumor microenvironment to regulate glutamine is through RASAL3 epigenetic silencing. More practically, therapeutic approaches targeting hormone signaling must consider these metabolic adaptations as means of resistance.

The precedence of PCa neuroendocrine differentiation associated with next generation ADT administration is a prominent manifestation of late stage disease (34, 46). However, mechanisms for ADT induction of neuroendocrine PCa are less well understood. An example involving paracrine IL-8 derived from neuroendocrine PCa cells was found to promote neuroendocrine differentiation (47). The impact of autocrine adrenomedullin and IL-6 in neuroendocrine differentiation is also described (48, 49). Here we defined an androgen-dependent mechanism for CAF-mediated neuroendocrine differentiation of adjacent prostatic epithelia. It is known that glutamine sensing triggers mTOR activity (50, 51). mTOR signaling is associated with PCa neuroendocrine differentiation (28, 52, 53). Therefore, we reasoned that targeting glutamine metabolism may serve as a therapeutic means of limiting neuroendocrine differentiation, in sensitizing PCa to ADT. Importantly, stromal glutamine was necessary and sufficient to promote PCa neuroendocrine differentiation (Figures 4-6). As ADT potentiated stromal glutamine secretion, combination therapy of castration/enzalutamide and targeting glutamine uptake by cancer cells with GPNA could serve as a viable synthetic lethal approach. This concept was corroborated by pharmacologic inhibition and knockdown of SLC1A5 by reducing neuroendocrine differentiation and dramatically reducing tumor size with ADT, compared to ADT alone in a mouse model of castrate resistant

disease (Figures 5, 6 and Supplemental Figure 5). Previous findings supported SLC1A5 to be highly expressed in PCa and breast cancer tissues and their inhibition led to reduced cell growth (51, 54). However, as this was the first demonstration of such a direct role the tumor microenvironment on promoting PCa neuroendocrine differentiation, we sought to validate the findings in PCa patient blood samples. Our data suggested that plasma glutamine can be used as a prognostic marker to follow ADT response and development of resistance (Figure 7). The importance of the work here involves the novel mechanism for ADT induced PCa neuroendocrine differentiation and further clinical validation through the measurement of plasma glutamine. Further, ADT can induce epigenetic alteration of the stromal fibroblasts to promote PCa neuroendocrine differentiation in glutamine dependent manner.

The elevated glutamine levels detected in the blood of patients on androgen deprivation therapy, suggest that nearly any metastatic site would be exposed to this amino acid in support of elevated energy needs as well as neuroendocrine differentiation. Adjuvant androgen deprivation therapy is commonly administered to patients with recurrent prostate cancer. As most PCa recurrence is local, the orthotopic grafts in our studies provide a relevant basis for blocking glutamine uptake and/or metabolism. As far as distant metastasis, one could extrapolate that local tumor expansion can affect distant metastatic progression via glutamine. Future studies could include testing the role of circulating glutamine on bone and visceral metastatic progression of PCa.

Methods

Cell Culture. Prostatic fibroblasts from prostate cancer patients and mouse prostates were cultured in high glucose Dulbecco's Modified Eagle Medium-F12 supplemented with 5% fetal bovine serum, 5% Nu-Serum, Antibiotic-Antimycotic (all from Fisher Scientific) and 10^{-9} M testosterone (55). In order to test the tumor inductive capacity of the primary human prostatic fibroblasts, they were xenografted with non-tumorigenic BPH1 prostatic epithelia (a kind gift of Simon W. Hayward, NorthShore University, Chicago IL) under the renal capsule, as previously described (8, 9). The fibroblasts were termed 'CAF' only if tumors developed in 4 weeks of grafting; otherwise, the non-tumor inductive fibroblasts were termed 'NAF'. CWR22Rv1 and C4-2B cells (American Type Culture Collection) were maintained in RPMI-1640 medium with 5% fetal bovine serum and 1% penicillin/streptomycin. All cultures were grown in a humidified 5% CO_2 environment at 37 °C.

DNA methylation analysis. Libraries were prepared from 200-500 ng of genomic DNA digested with 60 units of TaqαI and 30 units of MspI (NEB) sequentially and then extracted with Zymo Research DNA Clean & Concentrator™-5 kit. Fragments were ligated to pre-annealed adapters containing 5'-methyl-cytosine instead of cytosine according to Illumina's specified guidelines (www.illumina.com). Adaptor-ligated fragments of 150–250 bp and 250–350 bp in size were recovered from a 2.5% NuSieve 1:1 agarose gel (Zymo Research). The fragments were then bisulfite-treated using the EZ DNA Methylation-Lightning™ Kit. Preparative-scale PCR was performed, and the resulting products were purified for sequencing on an Illumina HiSeq. (Further details of DNA methalome analysis provided in Supplementary Material.)

Bisulfite Sequencing. Bisulfite sequencing was performed as described previously (56). Briefly, genomic DNA was extracted from the NAF and CAF samples and 200 ng of DNA was bisulfite converted by using the EZ DNA Methylation-Gold Kit (Zymo Research, Irvine, CA) according to the manufacturer's protocol. Three overlapping

primers were used for amplification of exon 2 region of RASAL3 by ZymoTaq DNA polymerase (Zymo Research) and subsequently cloned into the pCR2.1-TOPO vector (Invitrogen by Life Technologies, Carlsbad, CA). The primer sequences used to amplify the three regions were designed by using the Meth-Primer program (http://www.urogene.org/methprimer/) and are listed in Supplementary Table 6. Five clones from each sample were sequenced by using Sanger's method.

Macropinocytosis assay. Fibroblasts and PCa epithelia were grown on cover slips, serum-starved for 18 hours, prior to TMR-dextran (1 mg/ml; 70 kDa, FITC-labeled, Fisher Scientific) incubation for 30 min at 37 °C for macropinosomes labeling (18). After removing the dextran containing medium, cells were rinsed five times in cold PBS and fixed in 3.7% formaldehyde. Coverslips mounted in DAPI containing mounting medium (Vectashield) onto slides. Images were captured using laser confocal scanning microscopy (Leica) and analyzed via LASX software. To determine if the macropinosomes co-localize with lysosomes, LysoTracker Green (Fisher Scientific) was added in cells along with TMR dextran for 30 min. To determine whether the internalized albumin was degraded, we utilized a self-quenching fluorescent dye, DQ-BSA (10 μg/ml for 30 min), where lysosomal proteases enable fluorescent visualization by confocal microscopy.

3D organotypic co-culture. A modified version of the 3D organotypic co-culture system was performed in a collagen matrix similar to that previously reported (57). Matrix were prepared by mixing five volumes of rat tail collagen with two volumes of matrigel in one volume of 10x DMEM medium, and one volume of fetal bovine serum. CWR22Rv1 or C4-2B epithelia and primary mouse prostatic fibroblasts (WT or Ras^{V12}) were combined in a 1:3 ratio in the matrix. Nylon squares were coated with collagen and placed on metal grids in a 6-well plate. Matrix plugs containing cells, formed in 96 well plates (150 μl), were transferred onto the nylon squares and media was added to the level of the nylon mesh. Following treatments, the cells were dissociated from the matrix with collagenase and dispase for FACS analysis.

Seahorse XF-24 metabolic flux analysis. Oxygen consumption rate (OCR, pmol min−1) was measured with the Seahorse Bioscience XF24 extracellular flux analyzer. Cells were incubated in a CO_2-free incubator for 1 hr at 37 °C to allow for temperature and pH equilibration prior to loading into the XF24 apparatus. Initial assays were performed to optimize cell number, FCCP concentration and oligomycin concentration (data not shown). We used L-Glutamic acid γ-(p-nitroanilide) hydrochloride (GPNA, 10 μM; Sigma-Aldrich), a glutamine transporter inhibitor.

Spectral magnetic resonance for glutamine/glutamate. Chemical exchange saturation transfer effect of amine protons was used to image glutamine and glutamate, using a 9.4T micro-MRI in orthotopic prostate xenografts in mice, similar to that previously described (27). The mice were imaged before and one hour after intraperitoneal administration of the macropinocyosis inhibitor 5-(N-ethyl-N-isopropyl)amiloride (EIPA).

Tissue recombination mouse models. Cell recombinants were prepared by mixing $2x10^5$ epithelial (CWR22Rv1) cells with $6x10^5$ CAFs or stromal cells expressing Ras^{V12} per site in collagen as described before (6). Orthotopic grafting constituted the placing of the collagen plugs in the two anterior lobes of the prostate and kidney grafts were placed under the renal capsule of C57BL/6 male 8 week old mice, as described previously (3, 6). The mice were either left intact or castrated 1 week after grafting. The intact mice were randomly divided into two groups, where one received 3 mg/kg 5-(N-Ethyl-N-isopropyl) amiloride (EIPA; Sigma-Aldrich) intraperitoneal injection or vehicle control every other day for one week. Castrated mice were treated with enzalutamide (5 mg/kg) either alone or in combination with GPNA (10 mg/kg) for three weeks. The tumor volumes were measured using digital calipers and calculated using the following formula: length (mm) × width (mm) × width (mm) × 0.52. When the mice were sacrificed, and tumors were excised and photographed. Formalin-fixed, paraffin-embedded (FFPE) xenograft tumor tissue was sectioned and stained with hematoxylin

and eosin (H&E) and staining for chromogranin A, TUNEL, phosphorylated-histone H3 and phosphorylated-mTOR.

Statistics. Reduced Representation Bisulfite Sequencing BaseClear (Netherlands) performed quality control, sequence processing and mapping of sequence reads as per their 'EpiQuest Genome-wide Basic' service package. Sequence depth was determined per CpG dinucleotide as the number of reads where methylation status could be determined and CpGs with a depth less than 10 reads in either condition was excluded. Methylation status of the remaining CpGs was calculated as the percentage of methyl-cytosine in total cytosine. Heatmap was made using metaboanlyst (http://www.metaboanalyst.ca) software using top 25 genes analyzed by ANOVA.

Statistical significance of differences between control and experimental groups was assessed by unpaired Student's t test (Two-tailed); for multiple comparisons, one-way ANOVA was followed by Sidak multiple comparison tests. P-values reported in the manuscript were after Sidak correction for the multiplicity problem. The repeated-measures two-way ANOVA with post hoc analyses was also used where appropriate. *P* values of less than 0.05 were considered statistically significant. Data presented in figure legends is represented as mean ± SD unless otherwise stated; statistical tests utilized are reported in the figure legends, along with the associated *P* values.

Study approvals. All mouse studies were approved and performed by approved Cedars-Sinai Animal Care and Use Committee protocol. All PCa patients treated with ADT in this study, detailed in Table 1, were consented for blood analysis under Institutional Review Board of Cedars-Sinai Medical Center.

Author contributions

Conceptualization: RM and NAB; Methodology and Project Administration: RM; Investigation: RM, SH, VP, AM, PA, KR-R, FD, BA, SW, and MT; Formal Analysis: RM, FD, ZL; Writing: RM, RG, AM and NAB; Supervision and Funding, NAB, RG, EMP.

Acknowledgments

We thank the patients that contributed to this study. Matrigel was acquired from the National Cancer Institute/National Institute of Health Tumor Microenvironment Network. Spectral MR studies were performed at the Cedars-Sinai Imaging Institute with the support of the UCLA CTSI (UL1TR001881). This work was supported by grants from the National Cancer Institute (CA108646 and CA098912) and Veterans Affairs (BX001040) to NAB.

References

1. Siegel R, Ma J, Zou Z, and Jemal A. Cancer statistics, 2014. *CA Cancer J Clin.* 2014;64(1):9-29.

2. Ferlay J, Soerjomataram I, Dikshit R, Eser S, Mathers C, Rebelo M, Parkin DM, Forman D, and Bray F. Cancer incidence and mortality worldwide: sources, methods and major patterns in GLOBOCAN 2012. *Int J Cancer.* 2015;136(5):E359-86.

3. Placencio VR, Sharif-Afshar AR, Li X, Huang H, Uwamariya C, Neilson EG, Shen MM, Matusik RJ, Hayward SW, and Bhowmick NA. Stromal transforming growth factor-beta signaling mediates prostatic response to androgen ablation by paracrine Wnt activity. *Cancer Res.* 2008;68(12):4709-18.

4. Singh M, Jha R, Melamed J, Shapiro E, Hayward SW, and Lee P. Stromal androgen receptor in prostate development and cancer. *Am J Pathol.* 2014;184(10):2598-607.

5. Bianchi-Frias D, Basom R, Delrow JJ, Coleman IM, Dakhova O, Qu X, Fang M, Franco OE, Ericson NG, Bielas JH, et al. Cells Comprising the Prostate Cancer Microenvironment Lack Recurrent Clonal Somatic Genomic Aberrations. *Mol Cancer Res.* 2016;14(4):374-84.

6. Banerjee J, Mishra R, Li X, Jackson RS, 2nd, Sharma A, and Bhowmick NA. A reciprocal role of prostate cancer on stromal DNA damage. *Oncogene.* 2014;33(41):4924-31.

7. Zong Y, Huang J, Sankarasharma D, Morikawa T, Fukayama M, Epstein JI, Chada KK, and Witte ON. Stromal epigenetic dysregulation is sufficient to initiate mouse prostate cancer via paracrine Wnt signaling. *Proc Natl Acad Sci U S A.* 2012;109(50):E3395-404.

8. Olumi AF, Grossfeld GD, Hayward SW, Carroll PR, Tlsty TD, and Cunha GR. Carcinoma-associated fibroblasts direct tumor progression of initiated human prostatic epithelium. *Cancer Res.* 1999;59(19):5002-11.

9. Hayward SW, Wang Y, Cao M, Hom YK, Zhang B, Grossfeld GD, Sudilovsky D, and Cunha GR. Malignant transformation in a nontumorigenic human prostatic epithelial cell line. *Cancer Res.* 2001;61(22):8135-42.

10. Trimboli AJ, Cantemir-Stone CZ, Li F, Wallace JA, Merchant A, Creasap N, Thompson JC, Caserta E, Wang H, Chong JL, et al. Pten in stromal fibroblasts suppresses mammary epithelial tumours. *Nature.* 2009;461(7267):1084-91.

11. Bhowmick NA, Chytil A, Plieth D, Gorska AE, Dumont N, Shappell S, Washington MK, Neilson EG, and Moses HL. TGF-beta signaling in fibroblasts modulates the oncogenic potential of adjacent epithelia. *Science.* 2004;303(5659):848-51.

12. Cheng N, Bhowmick NA, Chytil A, Gorksa AE, Brown KA, Muraoka R, Arteaga CL, Neilson EG, Hayward SW, and Moses HL. Loss of TGF-beta type II receptor in fibroblasts promotes mammary carcinoma growth and invasion through upregulation of TGF-alpha-, MSP- and HGF-mediated signaling networks. *Oncogene.* 2005;24(32):5053-68.

13. He Y, Franco OE, Jiang M, Williams K, Love HD, Coleman IM, Nelson PS, and Hayward SW. Tissue-specific consequences of cyclin D1 overexpression in prostate cancer progression. *Cancer Res.* 2007;67(17):8188-97.

14. Valencia T, Kim JY, Abu-Baker S, Moscat-Pardos J, Ahn CS, Reina-Campos M, Duran A, Castilla EA, Metallo CM, Diaz-Meco MT, et al. Metabolic reprogramming of stromal fibroblasts through p62-mTORC1 signaling promotes inflammation and tumorigenesis. *Cancer Cell.* 2014;26(1):121-35.

15. Minciacchi VR, Spinelli C, Reis-Sobreiro M, Cavallini L, You S, Zandian M, Li X, Mishra R, Chiarugi P, Adam RM, et al. MYC Mediates Large Oncosome-Induced Fibroblast Reprogramming in Prostate Cancer. *Cancer Res.* 2017;77(9):2306-17.

16. Fiaschi T, Marini A, Giannoni E, Taddei ML, Gandellini P, De Donatis A, Lanciotti M, Serni S, Cirri P, and Chiarugi P. Reciprocal metabolic reprogramming through lactate shuttle coordinately influences tumor-stroma interplay. *Cancer Res.* 2012;72(19):5130-40.

17. Sotgia F, Martinez-Outschoorn UE, Pavlides S, Howell A, Pestell RG, and Lisanti MP. Understanding the Warburg effect and the prognostic value of stromal caveolin-1 as a marker of a lethal tumor microenvironment. *Breast Cancer Res.* 2011;13(4):213.

18. Commisso C, Davidson SM, Soydaner-Azeloglu RG, Parker SJ, Kamphorst JJ, Hackett S, Grabocka E, Nofal M, Drebin JA, Thompson CB, et al. Macropinocytosis of protein is an amino acid supply route in Ras-transformed cells. *Nature.* 2013;497(7451):633-7.

19. Perera RM, and Bardeesy N. Pancreatic Cancer Metabolism: Breaking It Down to Build It Back Up. *Cancer Discov.* 2015;5(12):1247-61.

20. Koochekpour S, Majumdar S, Azabdaftari G, Attwood K, Scioneaux R, Subramani D, Manhardt C, Lorusso GD, Willard SS, Thompson H, et al. Serum glutamate levels correlate with Gleason score and glutamate blockade decreases proliferation, migration, and invasion and induces apoptosis in prostate cancer cells. *Clin Cancer Res.* 2012;18(21):5888-901.

21. Afratis N, Gialeli C, Nikitovic D, Tsegenidis T, Karousou E, Theocharis AD, Pavao MS, Tzanakakis GN, and Karamanos NK. Glycosaminoglycans: key players in cancer cell biology and treatment. *FEBS J.* 2012;279(7):1177-97.

22. Schroder B. The multifaceted roles of the invariant chain CD74--More than just a chaperone. *Biochim Biophys Acta.* 2016;1863(6 Pt A):1269-81.

23. Vaishnavi A, Capelletti M, Le AT, Kako S, Butaney M, Ercan D, Mahale S, Davies KD, Aisner DL, Pilling AB, et al. Oncogenic and drug-sensitive NTRK1 rearrangements in lung cancer. *Nat Med.* 2013;19(11):1469-72.

24. Davidson SM, Jonas O, Keibler MA, Hou HW, Luengo A, Mayers JR, Wyckoff J, Del Rosario AM, Whitman M, Chin CR, et al. Direct evidence for cancer-cell-autonomous extracellular protein catabolism in pancreatic tumors. *Nat Med.* 2017;23(2):235-41.

25. Tardito S, Oudin A, Ahmed SU, Fack F, Keunen O, Zheng L, Miletic H, Sakariassen PO, Weinstock A, Wagner A, et al. Glutamine synthetase activity fuels nucleotide biosynthesis and supports growth of glutamine-restricted glioblastoma. *Nat Cell Biol.* 2015;17(12):1556-68.

26. Wilson M, Gill SK, MacPherson L, English M, Arvanitis TN, and Peet AC. Noninvasive detection of glutamate predicts survival in pediatric medulloblastoma. *Clin Cancer Res.* 2014;20(17):4532-9.

27. Cai K, Haris M, Singh A, Kogan F, Greenberg JH, Hariharan H, Detre JA, and Reddy R. Magnetic resonance imaging of glutamate. *Nat Med.* 2012;18(2):302-6.

28. Wu C, and Huang J. Phosphatidylinositol 3-kinase-AKT-mammalian target of rapamycin pathway is essential for neuroendocrine differentiation of prostate cancer. *J Biol Chem.* 2007;282(6):3571-83.

29. Qian ZR, Ter-Minassian M, Chan JA, Imamura Y, Hooshmand SM, Kuchiba A, Morikawa T, Brais LK, Daskalova A, Heafield R, et al. Prognostic significance of MTOR pathway component expression in neuroendocrine tumors. *J Clin Oncol.* 2013;31(27):3418-25.

30. Kalin TV, Wang IC, Ackerson TJ, Major ML, Detrisac CJ, Kalinichenko VV, Lyubimov A, and Costa RH. Increased levels of the FoxM1 transcription factor accelerate development and progression of prostate carcinomas in both TRAMP and LADY transgenic mice. *Cancer Res.* 2006;66(3):1712-20.

31. Andersson E, Arvidsson Y, Sward C, Hofving T, Wangberg B, Kristiansson E, and Nilsson O. Expression profiling of small intestinal neuroendocrine tumors identifies subgroups with clinical relevance, prognostic markers and therapeutic targets. *Mod Pathol.* 2016;29(6):616-29.

32. Chan DW, Hui WW, Wang JJ, Yung MM, Hui LM, Qin Y, Liang RR, Leung TH, Xu D, Chan KK, et al. DLX1 acts as a crucial target of FOXM1 to promote ovarian cancer aggressiveness by enhancing TGF-beta/SMAD4 signaling. *Oncogene.* 2017;36(10):1404-16.

33. Szklarczyk D, Morris JH, Cook H, Kuhn M, Wyder S, Simonovic M, Santos A, Doncheva NT, Roth A, Bork P, et al. The STRING database in 2017: quality-controlled protein-protein association networks, made broadly accessible. *Nucleic Acids Res.* 2017;45(D1):D362-D8.

34. Beltran H, Tomlins S, Aparicio A, Arora V, Rickman D, Ayala G, Huang J, True L, Gleave ME, Soule H, et al. Aggressive variants of castration-resistant prostate cancer. *Clin Cancer Res.* 2014;20(11):2846-50.

35. Jin H, Wang X, Ying J, Wong AH, Cui Y, Srivastava G, Shen ZY, Li EM, Zhang Q, Jin J, et al. Epigenetic silencing of a Ca(2+)-regulated Ras GTPase-activating protein RASAL defines a new mechanism of Ras activation in human cancers. *Proc Natl Acad Sci U S A.* 2007;104(30):12353-8.

36. McLaughlin SK, Olsen SN, Dake B, De Raedt T, Lim E, Bronson RT, Beroukhim R, Polyak K, Brown M, Kuperwasser C, et al. The RasGAP gene, RASAL2, is a tumor and metastasis suppressor. *Cancer Cell.* 2013;24(3):365-78.

37. Bechtel W, McGoohan S, Zeisberg EM, Muller GA, Kalbacher H, Salant DJ, Muller CA, Kalluri R, and Zeisberg M. Methylation determines fibroblast activation and fibrogenesis in the kidney. *Nat Med.* 2010;16(5):544-50.

38. Cairns P, Okami K, Halachmi S, Halachmi N, Esteller M, Herman JG, Jen J, Isaacs WB, Bova GS, and Sidransky D. Frequent inactivation of PTEN/MMAC1 in primary prostate cancer. *Cancer Res.* 1997;57(22):4997-5000.

39. Gravina GL, Marampon F, Piccolella M, Motta M, Ventura L, Pomante R, Popov VM, Zani BM, Pestell RG, Tombolini V, et al. Hormonal therapy promotes hormone-resistant phenotype by increasing DNMT activity and expression in prostate cancer models. *Endocrinology.* 2011;152(12):4550-61.

40. Cunha GR, Hayward SW, Wang YZ, and Ricke WA. Role of the stromal microenvironment in carcinogenesis of the prostate. *Int J Cancer.* 2003;107(1):1-10.

41. Prins GS, Birch L, and Greene GL. Androgen receptor localization in different cell types of the adult rat prostate. *Endocrinology.* 1991;129(6):3187-99.

42. Wise DR, and Thompson CB. Glutamine addiction: a new therapeutic target in cancer. *Trends Biochem Sci.* 2010;35(8):427-33.

43. Marshall AD, van Geldermalsen M, Otte NJ, Lum T, Vellozzi M, Thoeng A, Pang A, Nagarajah R, Zhang B, Wang Q, et al. ASCT2 regulates glutamine uptake and cell growth in endometrial carcinoma. *Oncogenesis.* 2017;6(7):e367.

44. Shih AY, Erb H, Sun X, Toda S, Kalivas PW, and Murphy TH. Cystine/glutamate exchange modulates glutathione supply for neuroprotection from oxidative stress and cell proliferation. *J Neurosci.* 2006;26(41):10514-23.

45. Rabinovich S, Adler L, Yizhak K, Sarver A, Silberman A, Agron S, Stettner N, Sun Q, Brandis A, Helbling D, et al. Diversion of aspartate in ASS1-deficient tumours fosters de novo pyrimidine synthesis. *Nature.* 2015;527(7578):379-83.

46. Beltran H, Tagawa ST, Park K, MacDonald T, Milowsky MI, Mosquera JM, Rubin MA, and Nanus DM. Challenges in recognizing treatment-related neuroendocrine prostate cancer. *J Clin Oncol.* 2012;30(36):e386-9.

47. Huang J, Yao JL, Zhang L, Bourne PA, Quinn AM, di Sant'Agnese PA, and Reeder JE. Differential expression of interleukin-8 and its receptors in the neuroendocrine and non-neuroendocrine compartments of prostate cancer. *Am J Pathol.* 2005;166(6):1807-15.

48. Aaronson DS, Muller M, Neves SR, Chung WC, Jayaram G, Iyengar R, and Ram PT. An androgen-IL-6-Stat3 autocrine loop re-routes EGF signal in prostate cancer cells. *Mol Cell Endocrinol.* 2007;270(1-2):50-6.

49. Fina F, Muracciole X, Rocchi P, Nanni-Metellus I, Delfino C, Daniel L, Dussert C, Ouafik L, and Martin PM. Molecular profile of androgen-independent prostate cancer xenograft LuCaP 23.1. *J Steroid Biochem Mol Biol.* 2005;96(5):355-65.

50. Tolhurst G, Zheng Y, Parker HE, Habib AM, Reimann F, and Gribble FM. Glutamine triggers and potentiates glucagon-like peptide-1 secretion by raising cytosolic Ca2+ and cAMP. *Endocrinology.* 2011;152(2):405-13.

51. Wang Q, Hardie RA, Hoy AJ, van Geldermalsen M, Gao D, Fazli L, Sadowski MC, Balaban S, Schreuder M, Nagarajah R, et al. Targeting ASCT2-mediated glutamine uptake blocks prostate cancer growth and tumour development. *J Pathol.* 2015;236(3):278-89.

52. Moore SR, Guedes MM, Costa TB, Vallance J, Maier EA, Betz KJ, Aihara E, Mahe MM, Lima AA, Oria RB, et al. Glutamine and alanyl-glutamine promote crypt expansion and mTOR signaling in murine enteroids. *Am J Physiol Gastrointest Liver Physiol.* 2015;308(10):G831-9.

53. Kanayama M, Hayano T, Koebis M, Maeda T, Tabe Y, Horie S, and Aiba A. Hyperactive mTOR induces neuroendocrine differentiation in prostate cancer cell with concurrent up-regulation of IRF1. *Prostate.* 2017;77(15):1489-98.

54. van Geldermalsen M, Wang Q, Nagarajah R, Marshall AD, Thoeng A, Gao D, Ritchie W, Feng Y, Bailey CG, Deng N, et al. ASCT2/SLC1A5 controls glutamine uptake and tumour growth in triple-negative basal-like breast cancer. *Oncogene.* 2016;35(24):3201-8.

55. Tuxhorn JA, McAlhany SJ, Dang TD, Ayala GE, and Rowley DR. Stromal cells promote angiogenesis and growth of human prostate tumors in a differential reactive stroma (DRS) xenograft model. *Cancer Res.* 2002;62(11):3298-307.

56. Haldar S, Dru C, Mishra R, Tripathi M, Duong F, Angara B, Fernandez A, Arditi M, and Bhowmick NA. Histone deacetylase inhibitors mediate DNA damage repair in ameliorating hemorrhagic cystitis. *Sci Rep.* 2016;6(39257.

57. Stark HJ, Baur M, Breitkreutz D, Mirancea N, and Fusenig NE. Organotypic keratinocyte cocultures in defined medium with regular epidermal morphogenesis and differentiation. *J Invest Dermatol.* 1999;112(5):681-91.

Table 1. Association of patient androgen targeted therapy responsiveness and plasma glutamine levels.

Patient	Rx	CRPC	PSA baseline	PSA on treatment	Outcome	Glutamine (μmol/L)
1	A	yes	16.4	6.4	Responsive	64.6
2	B+L	no	52.2	0.75	Responsive	198.4
3	L	no	1.6	0.2	Responsive	337.5
4	B	no	21.3	11.3	Responsive	458. 3
5	L	no	6.5	<0.1	Responsive	539. 8
6	A+A5	yes	9.2	0.1	Responsive	870.4
7	B+L	no	16.2	2.3	Responsive	901.9
8	L+T	no	10.7	0.2	Responsive	901
9	E	no	0.2	0.1	Responsive	903
10	B+L	no	0.2	0.1	Responsive	906.9
11	E	yes	284.7	344.3	Non-Responsive	1035
12	A+A5	yes	63.5	116.5	Non-Responsive	1037.6
13	L	yes	7.3	7.8	Non-Responsive	1305
14	E+R	yes	51.9	71.5	Non-Responsive	1338
15	A+A5	yes	218	522.3	Non-Responsive	1359
16	E	yes	0.8	<0.1	Responsive	1650
17	L	no	14.3	0.1	Responsive	1809.5
18	A	yes	28.5	26.2	Non-Responsive	2030
19	A+A5	yes	4.2	0.8	Responsive	2090
20	L	no	5.3	1.1	Responsive	2394
21	B+L+R	no	5.7	0.1	Responsive	2535
22	B+G	no	17.9	5.7	Non-Responsive	2982
23	A+A5	yes	61.5	19.8	Responsive	3184.4
24	A+R	yes	17.7	25.6	Non-Responsive	3613.5
25	B+L	yes	0.4	3.7	Non-Responsive	3751.1
26	L	yes	0.9	1.2	Non-Responsive	3870
27	E	yes	61.3	116.7	Non-Responsive	4369.8
28	B+L	yes	4.4	0.8	Non-Responsive	4989

Androgen targeted therapeutic treatment:

A – Abiraterone A5 – Apalutamide B - Bicalutamide
E – Enzalutamide G – Goserelin L – Leuprolide
R – Radiation T – Triptorelin

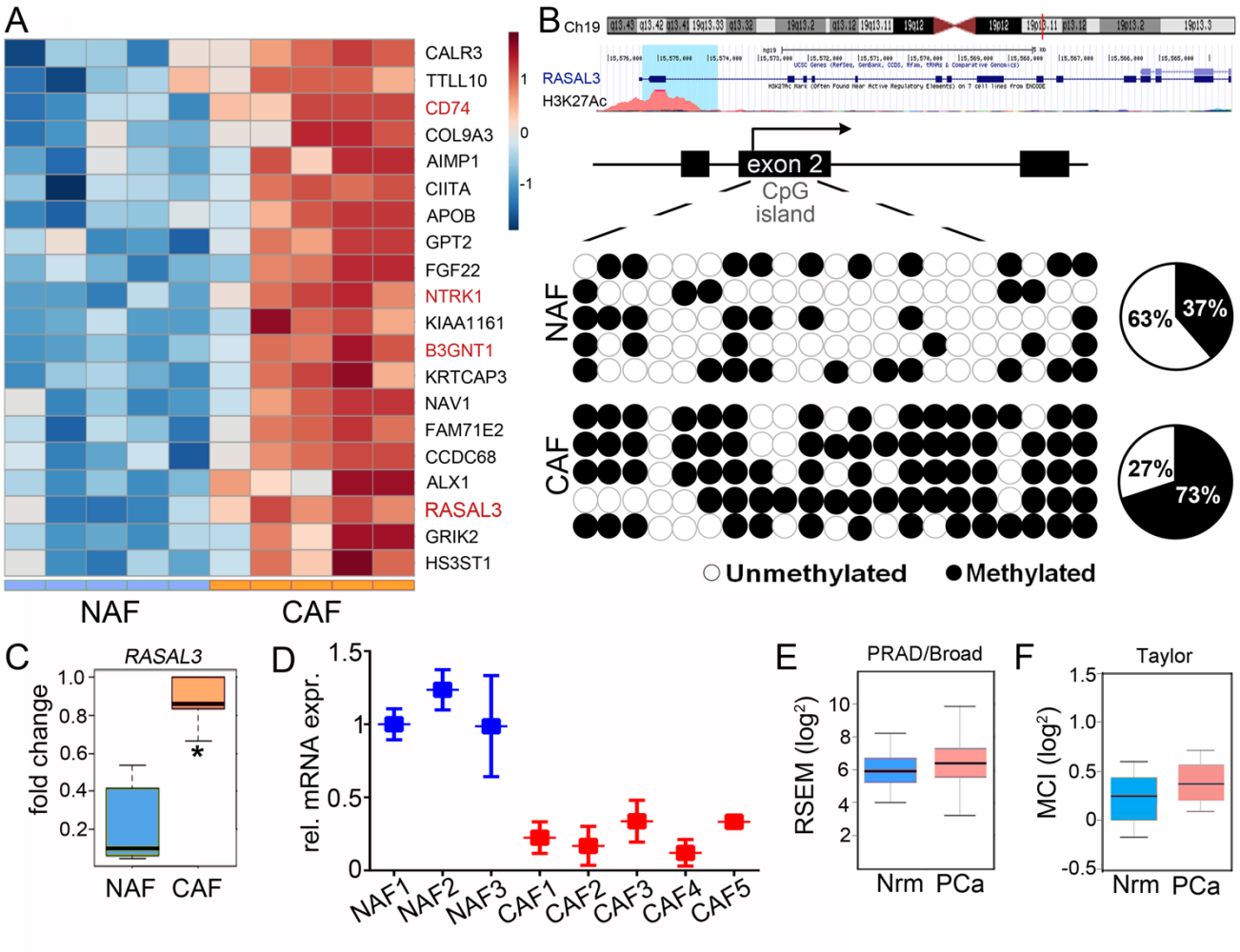

Figure 1. Epigenetic down-regulation of *RASAL3* in prostatic cancer associated fibroblast. **(A)** Heat map summarizing DNA methylation levels of CpG repeats (blue color indicates hypo-methylation and brown represents hyper-methylation). Top twenty methylated genes significantly differentially expressed between NAF and CAF. Each column represents a fibroblast sample and each row represents the methylation level of indicated gene (n=5). **(B) Top:** University of California at Santa Cruz Genome Browser screen shot of the indicated region of Chromosome 19 showing the positions of the *RASAL3* gene, histone 3 lysine 27 acetylation and human mRNA. **Bottom:** Locations of predicted CpG sites in Exon 2 by bisulfite sequencing, represented a filled (methylated) or empty circle (unmethylated, n = 5). The number of methylated CpGs divided by total number of true CpGs analyzed is given as a percentage on the pie chart. **(C)** Box plots representing the difference in

methylation state of the *RASAL3* gene promoter between NAF and CAF as measured by RRBS analysis (n=5). **(D)** *RASAL3* mRNA expression in a panel of primary fibroblast was examined by quantitative rtPCR, normalizing to *GAPDH* mRNA expression. **(E and F)** Box plots show relative gene expression level (log2) of the *RASAL3* in normal and prostate cancer patients from indicated data sets. Data represent the mean ± SD. **P* < 0.05 by two-tailed student's t test.

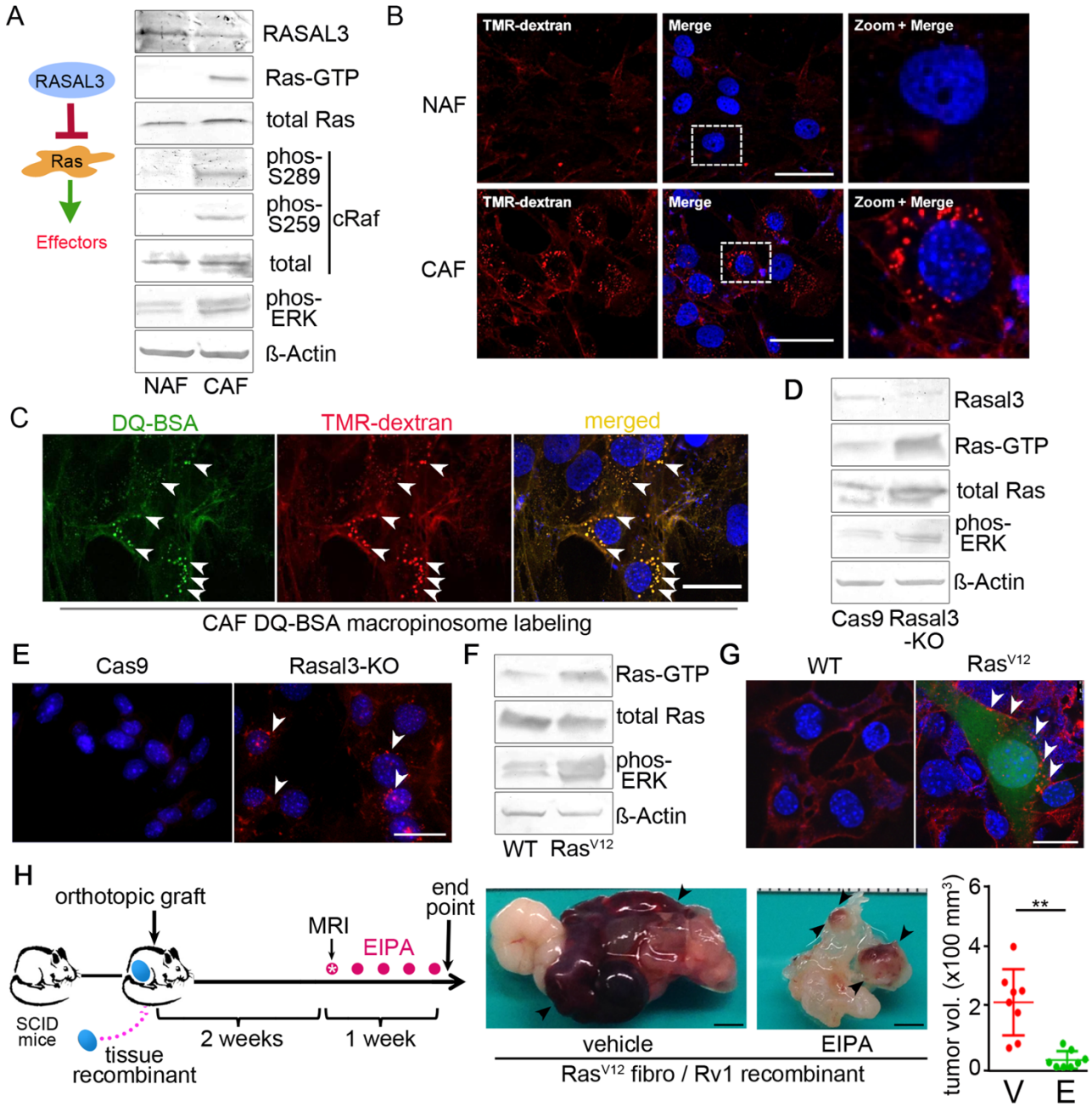

Figure 2. Ras activation stimulates macropinocytosis in prostatic fibroblasts and potentiates growth of adjacent epithelial. (A) Representative western blots of RASAL3, Ras, and Ras effectors in prostatic human NAF/CAF (n≥3). **(B)** TMR-dextran (red) uptake by CAF display elevated levels of macropinocytosis compared

to NAF. DAPI staining (blue) identifies nuclei. **(C)** CAF that were co-incubated with fluorescent DQ-BSA (green) and TMR-dextran (red) were fixed after 1 hr chase. The fluorescent signal emanating from DQ-BSA with TMR-dextran positive staining (arrowheads) indicate albumin uptake by macropinosomes and subsequent breakdown. (**D**) Representative western blots of RASAL3, total Ras, Ras-GTP, and phosphorylated-ERK expression by Rasal3-KO and Cas9 control mouse prostatic fibroblasts is shown (n≥3). (**E**) Representative images show TMR-dextran positive macropinosomes (arrowheads) in Rasal3-KO prostatic mouse fibroblasts compared to Cas9. (**F**) Representative western blots of mouse prostatic fibroblasts wild type (WT) and expressing Ras^{V12} indicate total Ras, Ras-GTP, and phosphorylated-ERK status (n≥3). **(G)** Representative images show TMR-dextran positive macropinosomes (arrowheads) in Ras^{V12} prostatic mouse fibroblasts (expressing GFP) compared to its WT counterpart. **(H)** Schematic illustrates orthotopic tissue recombinant xenograft models of CWR22Rv1 and Ras^{V12} mouse fibroblast allowed to grow for two weeks, followed by treatment with vehicle or 10 mg/kg EIPA (n=8). Representative gross tumor images are shown with a graph of all the tumor volumes. *P* value was calculated using two tailed student's t test. Data are represented as mean ± SD. ***P* < 0.01. Scale bars: 30 μm (B, C, E, G); scale bars: 3 mm (H).

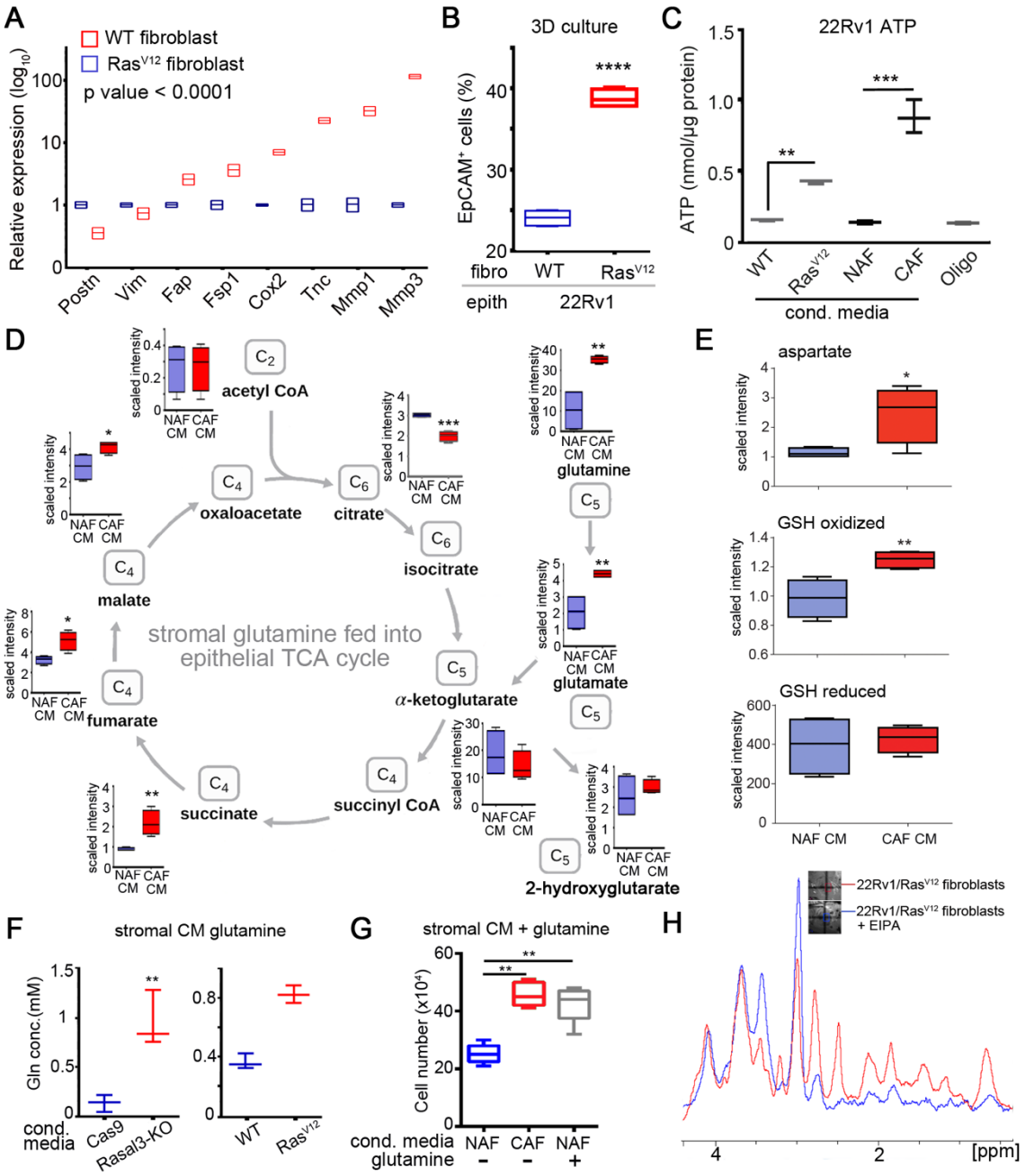

Figure 3. Ras activation in CAF drives glutamine metabolism in epithelia. (A) Relative mRNA expression levels of CAF-marker genes in WT and Ras^{V12} mouse fibroblast determined by quantitative rtPCR and analyzed using 2-way ANOVA (n≥3)**. (B)** EpCAM-positive cancer epithelial was quantitated by FACS of 3D co-cultures of human epithelial (CWR22Rv1) cells and WT or Ras^{V12} mouse fibroblasts. Statistical analysis was performed

using two-tailed student's t test (n≥3)**. (C)** ATP was measured in CWR22Rv1 after incubation with conditioned media human NAF or CAF or mouse WT or Ras^{V12} fibroblast or oligomycin in glutamine free media (n≥3). Statistical analysis was performed using 1-way ANOVA with multiple comparisons. **(D)** The diagram represents the TCA cycle in CWR22Rv1 cells treated with NAF- or CAF-conditioned media for 72 hours prior to metabolome analysis (n≥3)**. (E)** The metabolome analysis further indicated differential flux to aspartate, oxidized GSH, and GSH-reduced in CWR22Rv1 cells incubated with NAF- or CAF-conditioned media. **(F)** Glutamine concentrations were measured in the conditioned media from indicated mouse fibroblasts cultured for 72 hours. **(D-F)** Statistical analysis was performed using two-tailed student's t test (n≥3). **(G)** CWR22Rv1 proliferation was measured by cell counting following incubation with NAF and CAF conditioned media for 72 hrs in glutamine free media. NAF conditioned media was supplemented with 0.4 mM glutamine to mimic the glutamine levels expressed by CAF (see Supplemental Figure 4B). Statistical analysis was performed using 1-way ANOVA with multiple comparisons (n≥3). **(H)** Proton magnetic resonance spectroscopy data was acquired from orthotopically xenografted mice before and after EIPA administration. Spectra of the unfiltered data are superimposed using simulated echo acquisition (n = 3–4 per group). Glutamate, GLU; Glutamine, GLN; ppm, parts per million. **P* < 0.05, ***P* < 0.01, ****P* < 0.001, and *****P* < 0.0001.

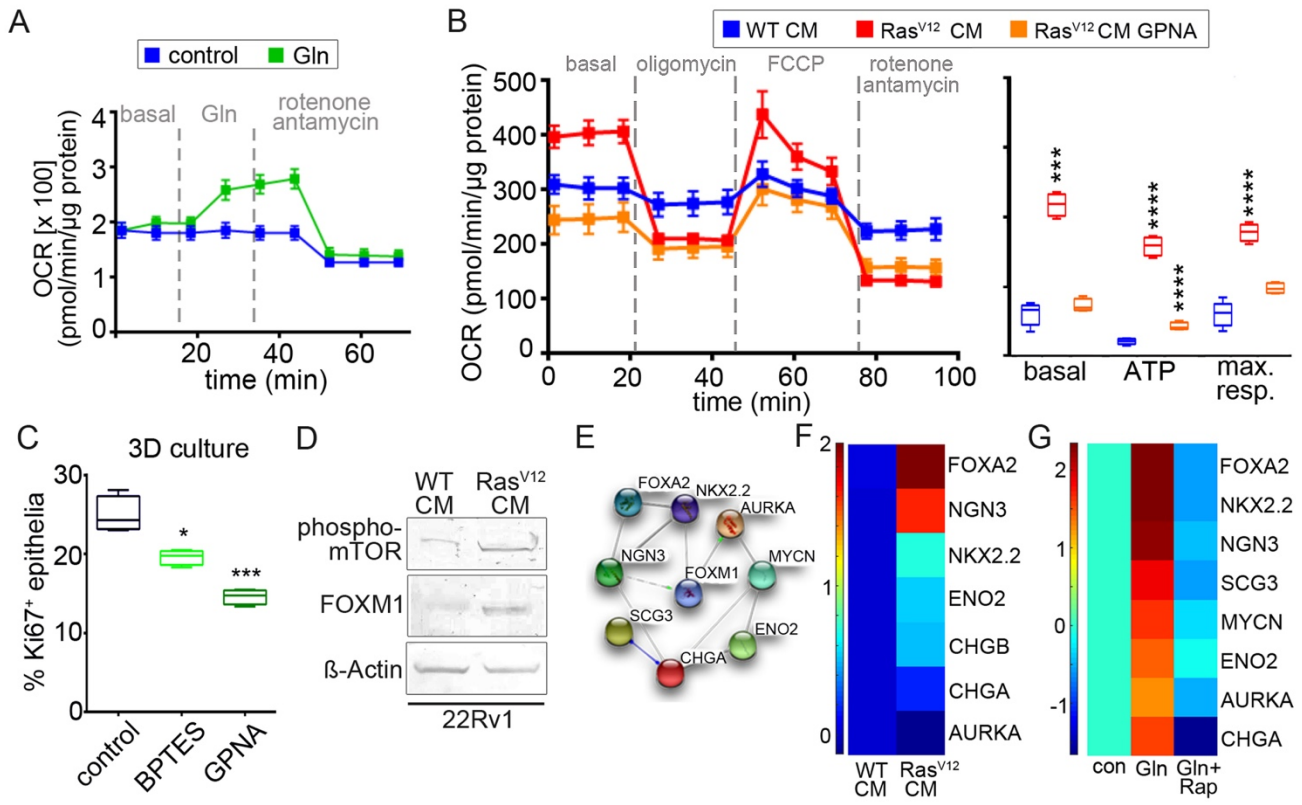

Figure 4. Stromal derived-glutamine induces mitochondrial bioenergetics and induction of PCa neuroendocrine differentiation. **(A)** Kinetic oxygen consumption rate (OCR) response in CWR22Rv1 cells exposed to 2 mM glutamine and rotenone along with antamycin. The OCR values were normalized to total protein. **(B)** Bioenergetic parameters of CWR22Rv1 cells incubated with wild type (WT)- or Ras^{V12}-fibroblast-conditioned media in the presence or absence of GPNA. **Left:** OCR trace for all three groups. **Right:** The basal OCR, ATP and maximal respiration are separately represented. Representative image of 3 independent experiments is shown. **(C)** CWR22Rv1 were co-cultured with WT- and Ras^{V12}-mouse prostatic fibroblasts in 3D, treated with vehicle, BPTES, or GPNA. Box plot of epithelial proliferation was measured by FACS analysis of $EpCAM^{+}/Ki67^{+}$ cells. Statistical analysis was performed using two tailed student's t test. **(D)** Phosphorylated-mTOR and FOXM1 protein levels were measured in CWR22Rv1 cells incubated with either WT- or Ras^{V12}-conditioned media for 3 days. **(A-D)** Representative image of 3 independent experiments is shown. **(E)** STRING

analysis of a PCa neuroendocrine gene signature demonstrates direct or indirect interactions with FOXM1. **(F)** Heatmap summarizing the qPCR results comparing the CWR22Rv1 expression of neuroendocrine marker genes following treatment with conditioned media from WT- or Ras^{V12}-fibroblasts or **(G)** L-glutamine alone in combination with rapamycin was compared to vehicle. Two-way ANOVA analysis indicates the overall *P* value with F-test $P < 0.0001$ for both experiments (n = 3; F, G). Epithelial and stromal cells were grown in glutamine free either DMEMF12 or RPMI media. Data are represented as mean ± SD. $*P < 0.05$, $***P < 0.001$, and $****P < 0.0001$.

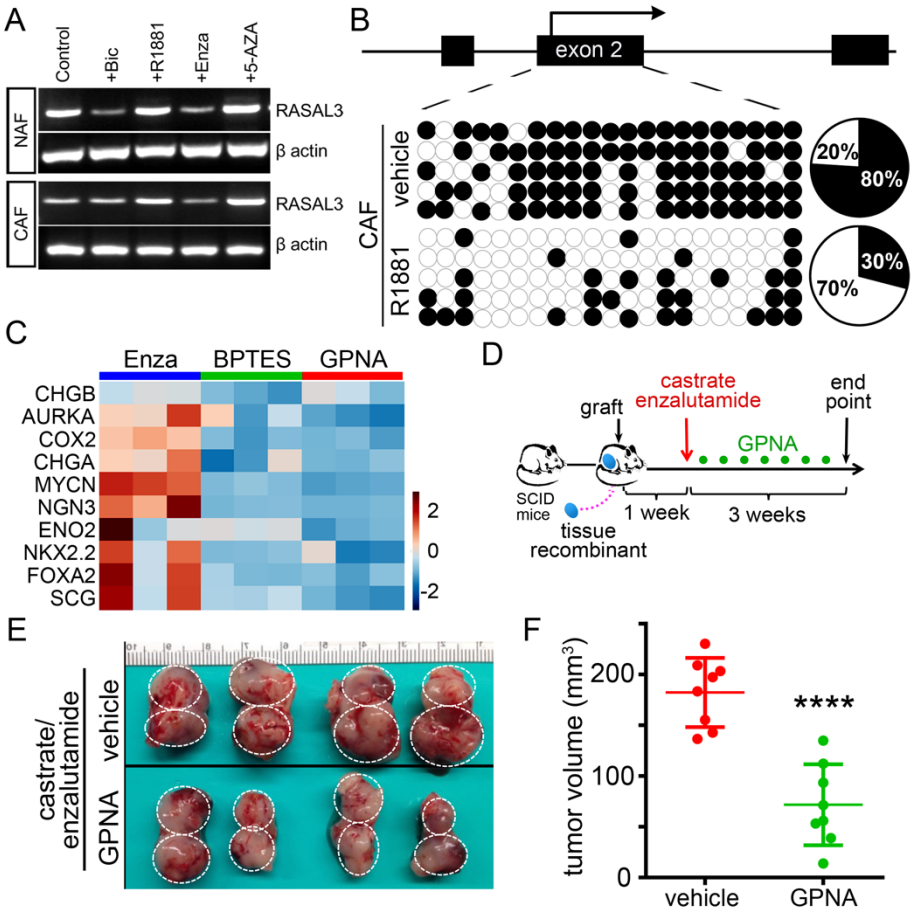

Figure 5. Androgen-mediated epigenetic regulation of *RASAL3* expression in CAF determines PCa neuroendocrine differentiation and tumor growth in castrate resistant xenograft models. (A) rtPCR analysis of *RASAL3* mRNA expression in NAF and CAF was performed following 5-day treatment with bicalutamide (Bic, 10^{-5} M), enzalutamide (Enza, 10^{-5} M), R1881 (10^{-9} M), or 5-Azacytadine (5-Aza, 5 mmol/L). ß-actin was used as a loading control. Representative image of 3 independent experiments is shown. **(B)** Bisulfide sequencing of the *RASAL3* exon 2 was performed on CAF following treatment with vehicle or R1881 for 5 days. The methylation status of the individual CpG dinucleotides is shown by unmethylated (empty) or methylated (filled) circles (n=5). **(C)** 3D co-cultures of human CWR22Rv1 with CAF were treated with vehicle, enzalutamide, BPTES, or GPNA for 3 days in glutamine free media and subjected to quantitative rtPCR for the expression of a neuroendocrine prostate cancer gene panel (n≥3, see Supplementary Table 4). Heatmap generated relative to

vehicle treatment. **(D)** Schematic diagram of the experimental design of castration, enzalutamide, and GPNA treatment of a castrate resistant xenograft model. Sub-renal capsule xenografts contained tissue recombinants of CWR22Rv1 and CAF. **(E)** Gross images of representative tumors (dashed circle) as shown on host kidneys. **(F)** Quantitated tumor volumes are represented as the mean ± SD, analyzed by two-tailed student's t test ($n \geq 8$). $^{**}P < 0.01$, $^{***}P < 0.001$, and $^{****}P < 0.0001$.

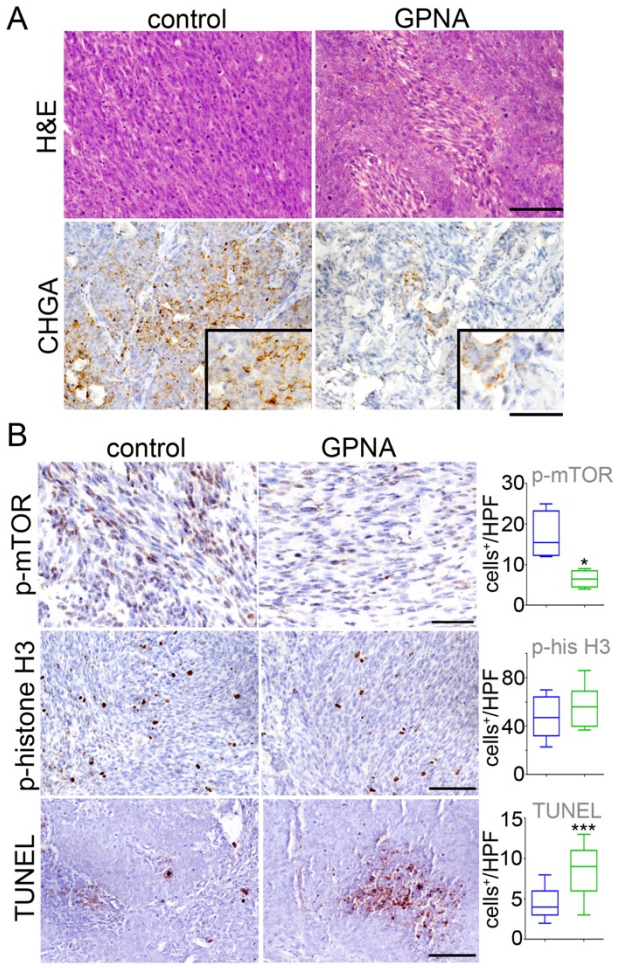

Figure 6. Glutamine uptake promotes tumor neuroendocrine differentiation and survival in the context of ADT. (A) H&E and chromogranin A (CHGA) staining of PCa xenografts indicate regulation by glutamine uptake antagonist, GPNA. **(B)** Representative staining for phosphorylated-mTOR, phosphorylated-histone H3 and TUNEL are shown for the PCa xenografts. Quantification of positive staining demonstrated significant differences when mice were treated with GPNA and ADT, compared to ADT alone. Scale bar represents 50 μm (n ≥ 8; A, B). Data represent the mean ± SD. Statistical analysis was performed using two tailed student's t test. *$P < 0.05$ and ***$P < 0.001$.

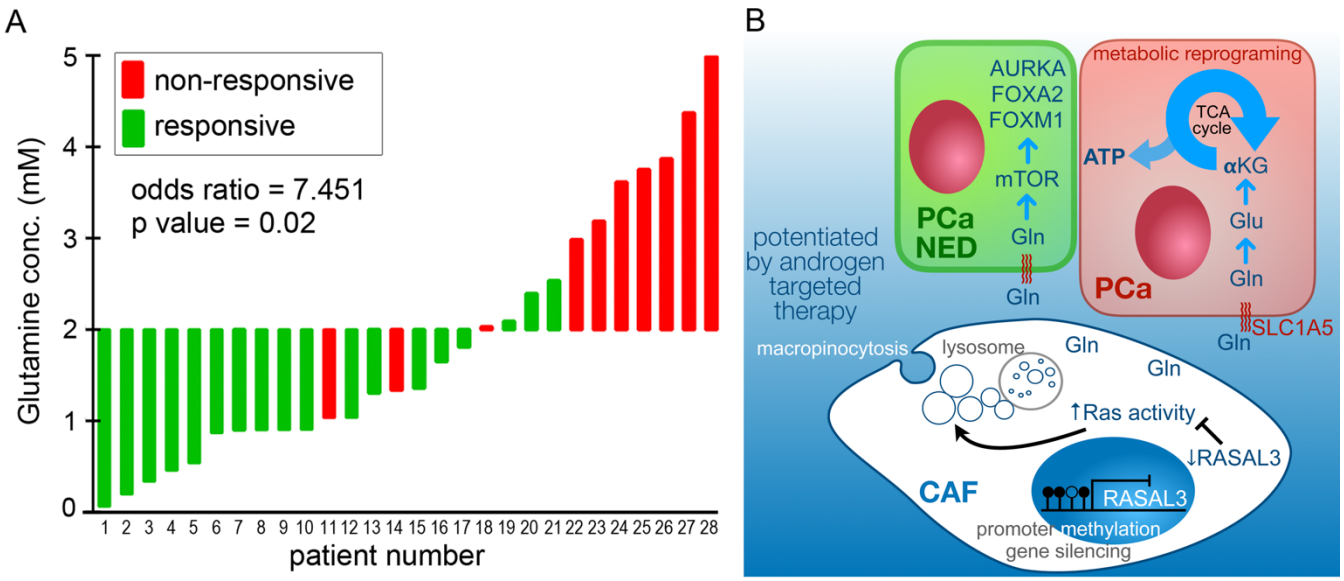

Figure 7. Sensitivity to androgen deprivation therapy correlates with blood glutamine levels is in support of a model of epigenetic Ras activation in prostatic fibroblasts and glutamine-mediated paracrine activity on prostate cancer epithelia. (A) Waterfall plot of plasma glutamine concentration in PCa patients on ADT correlated to therapeutic response (n = 28; see Table 1). Based on serum PSA detection, patients were determined to be responsive (green bars) and non-responsive (red bars) to ADT. The threshold of 2 mM glutamine was chosen as a determinant of ADT responsiveness. Fisher's exact test was used to determine odds ratio. **(B)** While RASAL3 promoter hypermethylation and gene silencing are observed in CAF compared to NAF, androgen targeted therapy furthers this epigenetic Ras activation process that induces macropinocytosis in stromal fibroblasts for the uptake of albumin. Albumin is degraded by the lysosomes to generate glutamine (Gln), shuttled into epithelia through glutamine transporter, SLC1A5. Glutamine is converted to glutamate (Glu) and α-ketoglutarate (αKG) in entering the TCA cycle in support of PCa epithelial proliferation. Glutamine also contributes to mTOR activation, leading to neuroendocrine differentiation (NED).